Title

Fully depleted charge-coupled device design and technology development

Journal

Astronomische Nachrichten, 344(8-9)

ISSN

0004-6337

Author

Holland, Stephen E

Publication Date

2023-10-01

DOI

10.1002/asna.20230072

Received: 27 April 2023 | Accepted: 28 April 2023

DOI: 10.1002/asna.20230072

Astronomische Nachrichten

PROCEEDING

Fully depleted charge-coupled device design and technology development

Stephen E. Holland

Physics Division, Lawrence Berkeley National Laboratory, Berkeley, California

Correspondence
Stephen E. Holland, Physics Division, Lawrence Berkeley National Laboratory, Berkeley, CA 94720, USA.
Email: seholland@lbl.gov

Funding information
U.S. Department of Energy; Director, Office of Science, Office of High Energy Physics of the U.S. Department of Energy, Grant/Award Number: DE-AC02-05CH11231; Office of the Director of National Intelligence, Grant/Award Number: D2021-2108030006; University of Chicago, Grant/Award Number: FP00011073; University of Washington, Grant/Award Number: FP00006742

Abstract

We describe the advancement of fully depleted charge-coupled device (CCD) technology for scientific applications. Recent efforts on 650–725 μm-thick CCDs for direct dark-matter and radiation detection with single-electron sensitivity are described, as well as the technology transfer of the fully depleted CCD technology to 200 mm-wafer fabrication facilities.

KEYWORDS

CCD, fully depleted, dark energy, dark matter, radiation detection, skipper CCDs

1 | INTRODUCTION

In this work, we describe the development of fully depleted charge-coupled devices (CCDs) for scientific applications in fields that include astrophysics, direct dark-matter detection, and fundamental radiation detection. The work is primarily sponsored by the United States Department of Energy (DOE), Office of Science, Office of High Energy Physics (HEP). The author's home institution, Lawrence Berkeley National Laboratory (LBNL), is a DOE Office of Science National Laboratory.

The CCDs described in this work consist of conventional CCD structures fabricated on high-resistivity, float-zone refined silicon (Holland et al. 2003). A substrate-bias voltage is applied to fully deplete the substrate. The substrate thickness ranges from about 200 to 725 μm depending on the application. The CCDs are operated at cryogenic temperatures, typically −140C. The majority of the CCD fabrication is done at Teledyne DALSA Semiconductor on 150 mm-diameter wafers with specialized processing for back-illuminated devices done at the LBNL MicroSystems Laboratory (Holland et al. 2007b).

The main advantage of the fully depleted CCD for astrophysics applications is the greatly improved quantum efficiency (QE) at red and near-infrared wavelengths that results from the large thickness (Groom et al. 2017). The absorption length in silicon increases strongly with wavelength, and fully depleted CCDs of hundreds of microns thickness are able to absorb near-infrared photons with high QE. The typical thickness for the astronomy CCDs we develop is 250 μm.

For direct dark-matter detection, the mass of the detecting medium should be as large as practical. As shown later, improvements in the silicon-substrate resistivity as well as advanced device designs for high-voltage operation have resulted in the full depletion of CCDs that are 650 – 725 μm thick for dark-matter detection. The use of thick CCDs as radiation detectors results in an improved detection efficiency for energetic γ and x-rays.

For astrophysics applications, the CCDs are back-illuminated to increase the QE. As discussed later, back illumination is also desirable for radiation detection in order to detect low-energy particles and x-rays.

The organization of this paper is as follows. We begin with a review of the CCDs developed for astrophysics, followed by a discussion of CCDs for direct dark-matter detection. We then discuss the development of a fully depleted, Skipper CCDs with sub-electron readout noise including methods to increase the readout speed for Skipper CCDs. We then describe our efforts to produce CCDs for radiation detection and our work to fabricate CCDs on high-resistivity, 200 mm-diameter wafers.

2 | FULLY DEPLETED CCDS FOR DOE DARK ENERGY EXPERIMENTS

The CCDs described here were first employed in significant numbers for the DOE Stage-III Dark Energy Survey. The main DOE role in this project was the delivery of the 570 Mpixel Dark Energy Camera (DECam). Fermi National Accelerator Laboratory (Fermilab) was the lead institution for DECam. The details of the DECam design and performance are reported in (Flaugher et al. 2015).

Figure 1a shows a picture of a 150 mm-diameter wafer with four 8 Mpixel CCDs and one 4 Mpixel device. The format for the 8 Mpixel CCD was 2048 (columns) × 4096 (rows) with (15 μm)^2 pixels. A picture of the completed camera is shown in Figure 1b. Each rectangular object in the figure is a back-illuminated, 8 Mpixel CCD. There are 62 imaging, 4 guider, and 8 alignment CCDs in the focal plane.

The Dark Energy Survey saw its "first light" in September 2012, and as of the time of this report has produced over 1.1 million images. The performance of the CCDs as of early 2019 is described in (Diehl 2020). The performance of the CCDs has been reliable with one permanent CCD failure, one noisy amplifier not used for science, and several anomalies that curiously resolved over time (Diehl 2020).

In December 2019, the DOE Stage-IV Dark Energy Spectroscopic Instrument (DESI) project began taking data with science operations starting in May of 2021 (Abareshi et al. 2022). There are 10 spectrographs in DESI each with 3 4k × 4k, (15 μm)^2 pixel CCDs.

For the blue wavelengths, the CCDs are thinned devices from Semiconductor Technology Associates (STA) and the University of Arizona Imaging Technology Laboratory. Fully depleted devices supplied by LBNL and Teledyne DALSA Semiconductor are used for the red and near-infrared wavelengths for a total of 20 fully depleted CCDs. As in DECam, the DESI CCDs are 250 μm thick. 500 μm-thick fully depleted CCDs were considered for the near-infrared spectrographs, but were not chosen due to the larger number of pixels per image lost due to

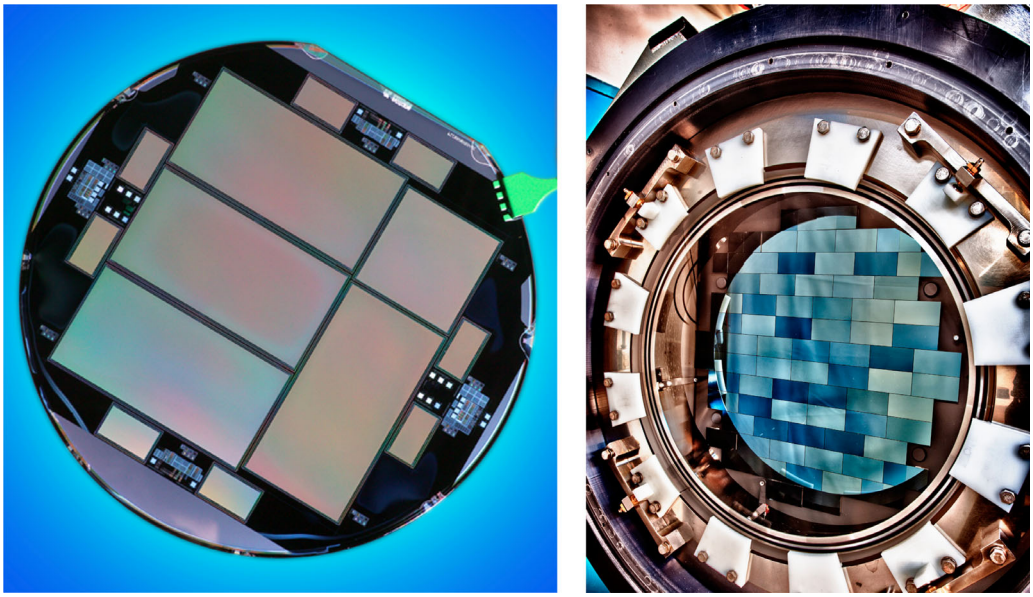

FIGURE 1 (a) A picture of a DECam CCD wafer. The diameter is 150 mm. (b) A picture of the completed focal plane for the Dark Energy Survey.

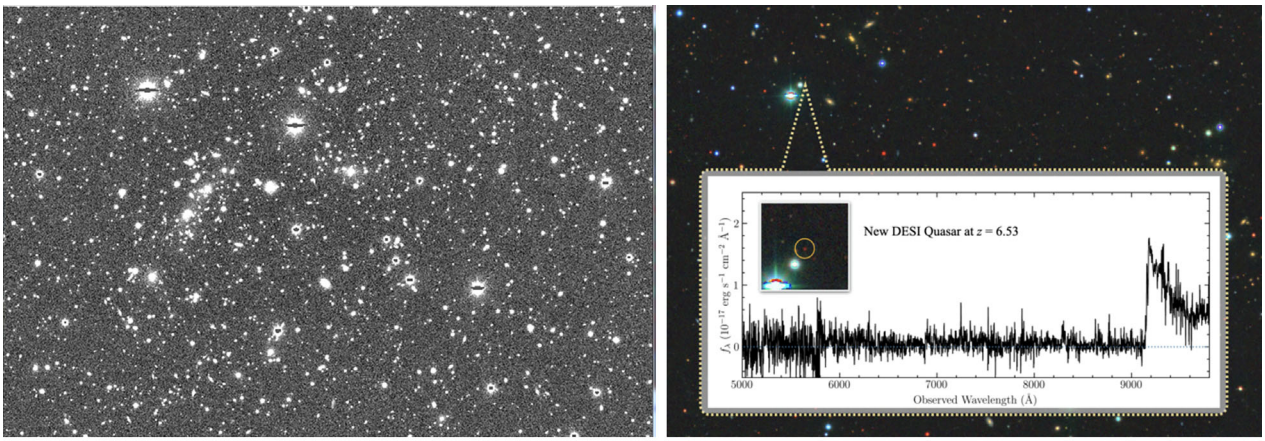

FIGURE 2 (a) A DECam image taken in the z-band (courtesy of T. Diehl, Fermilab). (b) A high-redshift quasar spectrum from DESI.

cosmic-ray muons and Compton electrons from environmental radiation (Smith et al. 2002). 500 μm-thick CCDs were employed in the Mayall 4-m telescope MOSAIC3 camera (Dey et al. 2016), and then repurposed for the Keck Telescope LRIS spectrograph (Kassis et al. 2022). The improvement in near-infrared QE for the 500 μm CCDs is reported in (Bebek et al. 2012).

As mentioned earlier, the main advantage of thick, fully depleted for astronomical applications is the high near-infrared QE (Holland et al. 2003). Also, the 10–20 μm-thick scientific CCDs such as the STA devices mentioned above suffer from fringing due to multiply-reflected light when the absorption depth exceeds the CCD thickness (Groom et al. 1999). Figure 2 shows a long-wavelength image taken with DECam as well as a spectrum of a high-redshift quasar measured with DESI. The DECam image was taken in the z-band, that is, the wavelength range of 800 to 1000 nm. The emission peak in the DESI quasar spectrum corresponds to the Lyman-α emission that has been redshifted from the rest wavelength of 121.567 nm to slightly over 900 nm. At these long wavelengths, the use of thinned scientific CCDs would be impractical due to low QE and fringing.

The DESI CCDs have improved performance over that of the DECam devices in terms of QE (Groom et al. 2017), read noise, and reduced artifacts due to the large pixel aspect ratio inherent to fully depleted CCDs (Bebek et al. 2017). The DESI CCDs also incorporate the high-voltage compatibility features discussed in more detail in Section 3.

Table 1 shows the read noise of the DESI CCDs measured at Kitt Peak in June of 2022.[1] Each entry in the table corresponds to the average read noise for the 4 amplifiers in each CCD. The overall average read noise for the fully depleted CCDs is 2.6 e$^-$ rms at an integration time of 4 μsec each for the baseline and signal.

[1]Data courtesy of J. Guy, LBNL.

TABLE 1 The measured read noise for the DESI CCDs as of June 2022. The number reported is the average of the 4 amplifiers in each CCD. The integration time was 4 μs each for the baseline and signal. The Red and NearIR results are for fully depleted CCDs.

DESI CCD read noise (e$^-$ rms)			
#	Blue	Red	NearIR
0	3.62	2.61	2.49
1	3.82	2.77	2.82
2	3.21	3.02	2.38
3	3.24	2.60	2.91
4	3.37	2.73	2.50
5	3.64	2.95	2.45
6	3.37	2.63	2.32
7	3.03	2.40	2.49
8	3.20	2.52	2.48
9	3.14	2.47	2.44

3 | FULLY DEPLETED CCDS FOR DARK MATTER DETECTION

Estrada et al. proposed the use of DECam fully depleted CCDs for direct dark-matter detection (Estrada et al. 2008). The CCD readout noise of a few electrons reduces the

low-energy threshold for dark-matter detection and the volume for detection was enhanced by about a factor of 10 comparing DECam CCDs to thinned scientific CCDs. Rejection of unwanted background events from environmental radioactivity is enhanced by the particle identification possible via the event spatial signature in combination with the measurement of the energy deposited per event. Also, the detection of individual atoms of U in the silicon substrate has been demonstrated by spatial correlation of events with energy deposits corresponding to the radioactive decay chain (Aguilar-Arevalo et al. 2015).

The DECam CCDs were not ideal for the dark-matter detection work due to the presence of an indium-tin-oxide anti-reflecting coating that is slightly radioactive. Also, it was desirable to increase the thickness beyond the 250 μm value used for the DECam CCDs. The maximum CCD thickness is limited by the thickness of the starting silicon that is 675 and 725 μm for 150 and 200 mm-diameter wafers, respectively. These thickness values are according to the SEMI Standards, where SEMI is a global industry association that sets standards for the semiconductor industry.

The depletion voltage for the fully depleted CCDs goes as the square of the thickness and inversely with the resistivity of the starting silicon. The capability to fully deplete standard thickness CCDs hinges on the ability to apply higher substrate-bias voltages than was the case for DECam, and would also benefit from improvements in the resistivity of the starting silicon.

CCD device designs for high-voltage compatibility were originally developed to safely operate (10.5 μm)^2 pixel, fully depleted CCDs that required high spatial resolution (Holland et al. 2006, 2009). The spatial resolution is determined by the lateral diffusion of the holes as they drift through the substrate to the CCD collection electrodes. The diffusion is minimized by decreasing the carrier transit time by increasing the electric field in the silicon substrate via higher substrate-bias voltages (Fairfield et al. 2006). Figure 3 shows a test-pattern image as well as measurements of background events for a 30-minute exposure under dark conditions for a high-voltage compatible CCD with a format of 3.5 k × 3.5 k with (10.5 μm)^2 pixels and operated with a substrate-bias voltage of 200 V. The CCD was completely fabricated at Teledyne DALSA Semiconductor, and the substrate resistivity and thickness were about 5000 Ω-cm and 650 μm, respectively. The latter is slightly thinner than the standard thickness of 675 μm due to the need to repolish the front sides of the wafers after an in-situ doped (phosphorus) polysilicon-gettering layer is deposited on the back sides of the wafers (Holland et al. 2007a).

In addition to the improved high-voltage capabilities of the CCD designs, there has been significant improvement in the substrate resistivity as seen in Table 2.

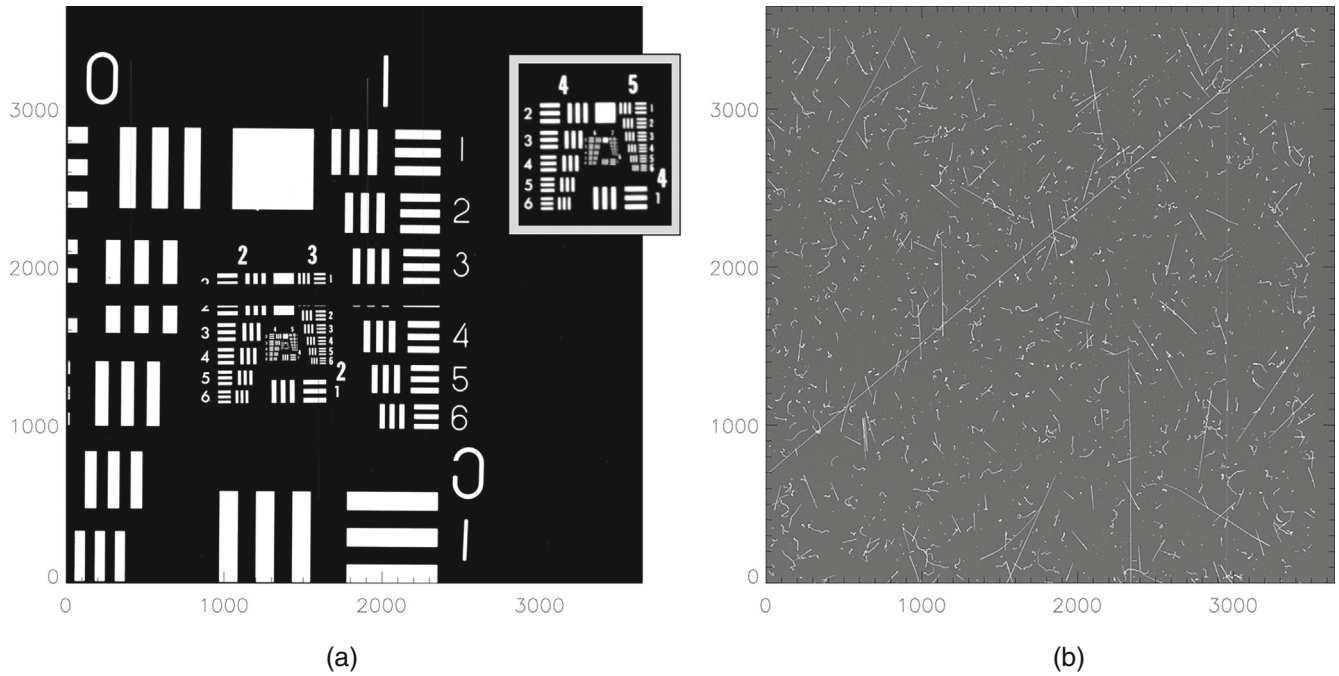

FIGURE 3 (a) An image taken by projecting a test pattern onto the CCD. The inset shows a magnified view of the test patterns at the center of the image. (b) Background events seen on the same CCD as in (a) after a 30-minute exposure under dark conditions. The operating temperature was −140C, and the substrate bias voltage was 200V. The substrate resistivity was about 5000 Ω-cm.

In 2009 the resistivity of crystals acquired at LBNL was in the 5000 – 7000 Ω-cm range. Since then silicon with resistivity greater than 20,000 Ω-cm is readily available, and this translates into about a factor of four less voltage required for full depletion when compared to the older 5000 Ω-cm material. Also shown in Table 2 is the photoconductive-decay lifetimes that are related to the generation lifetime. The CCD dark current is inversely proportional to the generation lifetime that is a measure of the purity of the silicon with respect to contaminants that can introduce deleterious mid-gap states (Grove 1967). The mid-gap states due to for example Fe and Au are efficient generators of dark current (Claeys & Simoen 2018).

TABLE 2 Resistivity and photoconductive-decay lifetime for various batches of Topsil silicon wafers acquired at LBNL. The last two rows in the table are for 200 mm-diameter wafers. All previous entries refer to 150 mm-diameter wafers.

Silicon resistivity and lifetime			
Year	**Topsil Crystal**	**Resistivity (k Ω − *cm*)**	**Lifetime (ms)**
2009	2142946	5.5–7	4.4
2009	2143310	5.0–6	16.3
2009	2144322	14–20	3.4
2014	22-0572-10	20–28	21.4
2015	33-0203-20	22–26	21.4
2019	31-1062-10	>10	22.4
2020	33-1751-30	>10	18.9
2020	32-1345-20	18–20	23.5
2020	34-1802-10	17.7–22.4	18.4

4 | SKIPPER CCD RESEARCH AND DEVELOPMENT

In the fall of 2009 J. Estrada of Fermilab communicated with the author regarding the possibility of producing fully depleted CCDs with "Skipper" amplifiers. Fortuitously a new processing run at Teledyne DALSA Semiconductor was about to begin that included a Skipper CCD design. The email correspondence is reproduced in Figure 4 along with a picture of a finished wafer that included the first fully depleted Skipper CCDs produced by LBNL.

The Skipper CCD concept was invented by Janesick (U.S. Patent 5250824) and relies on the averaging of many reads of the charge packet via a non-destructive readout method. The latter is realized with a floating-gate amplifier where the signal charge is multiply sensed via an extension of the output source-follower gate electrode above the CCD channel, that is, the floating-gate electrode. For statistically independent sampling the read noise decreases as the inverse of the square root of the number of reads. The initial work by Janesick and collaborators on the Skipper CCD resulted in a minimum noise level of 0.5 e^- rms after 512 samples (Chandler et al. 1990; Janesick et al. 1990). No further improvement in the noise was noted for more sampling implying systematic effects. The ability to achieve sub-electron read noise would be of great value for direct dark-matter detection experiments.

The floating-gate amplifier concept was introduced in 1973, and exploitation of the non-destructive readout capability was mentioned in the context of a proposed "distributed floating-gate amplifier" where the charge would be sensed by multiple amplifiers (Wen & Salsbury 1973). The first experimental results were presented shortly after the initial publication (Wen 1974), and

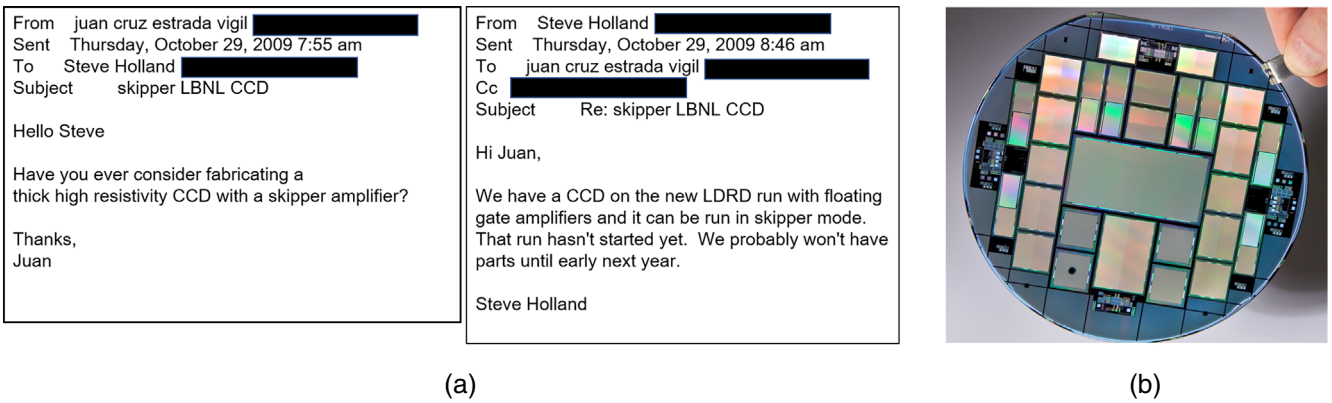

FIGURE 4 (a) Electronic mail correspondence between J. Estrada of Fermilab and the author in the fall of 2009. (b) A picture of the completed wafer referred to in the email correspondence of (a). Numerous designs were employed on this wafer including the first prototype fully depleted Skipper CCD produced by LBNL.

this was followed by the demonstration of the readout of a CCD with a distributed floating-gate amplifier (Wen et al. 1975).

The first fully depleted Skipper CCD we produced with Teledyne DALSA Semiconductor was tested at Fermilab and achieved 0.2 e^- rms after 1227 samples (Fernández Moroni et al. 2012). The high-voltage device design methods cited earlier were incorporated into this CCD. Our second generation Skipper CCD was demonstrated to have a noise of 0.068 e^- rms after 4000 samples (Tiffenberg et al. 2017). Figure 5a shows single-electron resolution for the second generation Skipper CCD that was exposed to a low-level light signal.

The prototype Skipper CCDs we developed were small-format devices. The design used for the second prototype was reformatted to produce two types of large-area CCDs for the Sub-Electron-Noise Skipper CCD Experimental Instrument (SENSEI) project. The formats were 6144 (columns) ×1024 (rows), and 866 (columns) × 6144 (rows). The pixel size was $(15\ \mu m)^2$ in both cases. Figure 5b shows the 6 die per wafer after dicing of a wafer fabricated at Teledyne DALSA Semiconductor into the individual CCDs with the outer parts of the diced wafer removed. The substrate resistivity was about 20,000 Ω-cm, and the approximately 650 μm-thick wafers were completely processed at Teledyne DALSA Semiconductor. The performance of the CCDs for direct dark-matter detection is described in (Barak et al. 2020).

The single-electron generation rate was reported to be $(1.5940 \pm 0.160 \times 10^{-4})$ e^-/pixel/day (Barak et al. 2020). This rate includes the bulk dark current due to electron-hole pair generation via mid-gap states, and the measured rate is about 5 orders of magnitude smaller than the few e^-/pixel/hour measured on the DECam and DESI CCDs. A major difference in the two applications is the infrared shielding in the case of SENSEI where the CCDs are enclosed in cold Cu vessels (Barreto et al. 2012). The thick, fully depleted CCDs are sensitive to near-infrared photons from 300K blackbody radiation as a result of the high-quantum efficiency out to wavelengths of about 1 μm (Bebek et al. 2012).

A detailed study of the various mechanisms contributing to the single-electron generation rate found that the rate mentioned above was at least an order of magnitude higher than that expected from the bulk dark current (Barak et al. 2022). A correlation of the single-electron generation rate with high-energy events was also noted in (Barak et al. 2020). Du et al. describe mechanisms that could account for the higher single-electron rate including Cherenkov photons from high-energy events such as cosmic-ray muons (Du et al. 2022).

In terms of the CCD technology, the bulk dark current is greatly reduced by the in-situ doped (phosphorus) polysilicon-gettering layer that is applied to the back side of the silicon as one of the first steps in the process (Holland 1989). The practical details concerning the implementation of this gettering method for fully depleted CCDs is described in (Holland et al. 2007a).

Figure 5c shows a wafer produced at Teledyne DALSA Semiconductor for the DArk Matter in CCDs at Modane (DAMIC-M) experiment (Arnquist et al. 2022). As was the case for the SENSEI CCDs, the second prototype Skipper CCD was reformatted in this case to 6144 (columns) × 1536 (rows) with $(15\ \mu m)^2$ pixels. The 1 kg-scale DAMIC-M experiment requires 200 CCDs, and fabrication has begun at Teledyne DALSA Semiconductor. SENSEI is a 100 g-scale experiment.

To summarize this section, the realization of thick, fully depleted CCDs with sub-electron noise is a significant advancement in the use of CCDs for direct dark-matter detection. The main drawback of the CCDs described in this section is the long readout time. In the following section, we describe R&D efforts to increase the readout speed of Skipper CCDs.

5 | IMPROVEMENTS IN THE READOUT SPEED FOR SKIPPER CCDS

We have pursued methods to increase the readout speed of Skipper CCDs under the auspices of the DOE Quantum Information Science (QIS) initiative. Figure 6a shows a picture of a 150 mm diameter wafer fabricated at Teledyne DALSA Semiconductor with various Skipper CCD designs labeled. In addition, we have produced our first 250 μm thick, back-illuminated Skipper CCDs from this batch of wafers by employing the hybrid fabrication production model used for the DECam and DESI CCDs (Holland et al. 2007b). Back illumination is necessitated by the requirement of high QE for the QIS applications.

The Skipper CCDs for dark-matter detection described in Section 4 have a single Skipper amplifier located at each of the four corners of the CCD. We modified a prior CCD design that had 16 conventional floating-diffusion amplifiers spaced every 512 columns (Bebek et al. 2012; Holland et al. 2014). The CCDs labeled "16 channel" in Figure 6a with a format of 4096 (columns) × 2048 (rows) and pixel size of $(10.5\ \mu m)^2$ were modified from the original with the floating-diffusion amplifiers replaced with Skipper amplifiers. Figure 6b shows a magnified view of one of the amplifier regions. Each amplifier reads out a 512-pixel serial register that is on a 10.2 μm pitch in order to accommodate the space needed for the Skipper amplifier. The lower

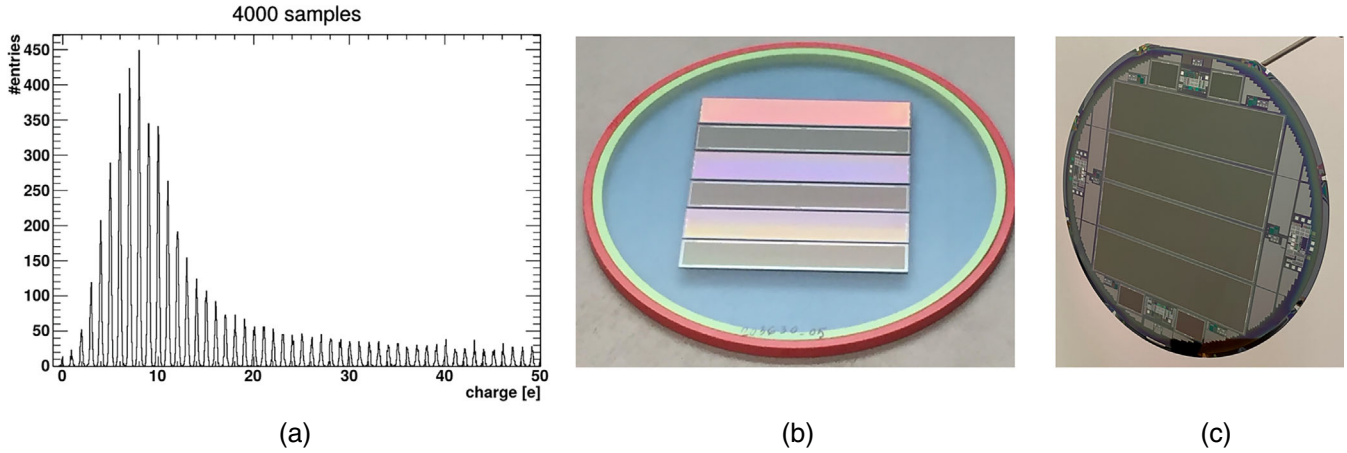

FIGURE 5 (a) A histogram of the measured charge obtained under low-level light conditions with the second prototype Skipper CCD described in the text. The figure is courtesy of J. Tiffenberg of Fermilab. (b) A picture of a SENSEI wafer after dicing the wafer into the individual CCDs. The CCD formats are 6144 (columns) ×1024 (rows) and 866 (columns) × 6144 (rows) with (15 μm)^2 pixels. (c) A picture of a DAMIC-M wafer. The CCD format is 6144 (columns) × 1536 (rows) with (15 μm)^2 pixels.

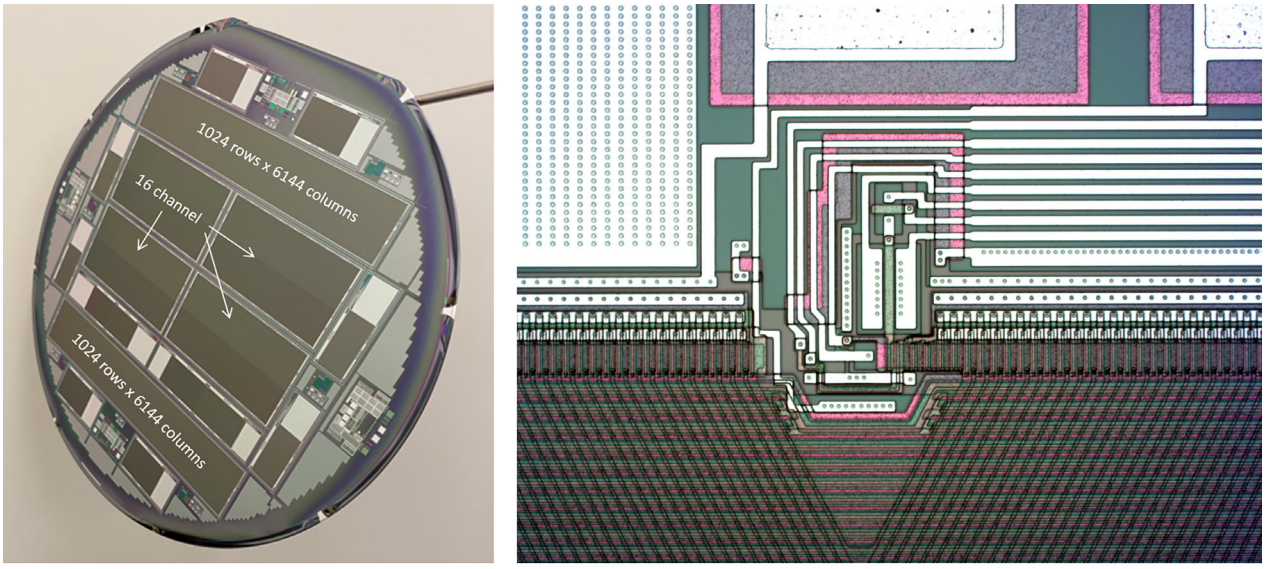

FIGURE 6 (a) A picture of a 150 mm diameter wafer that includes prototype Skipper CCDs for faster readout. (b) A picture showing the amplifier region of one of the 16-channel CCDs of (a). For scale, the series of horizontal and parallel Al lines on the right side of the picture are 20 μm wide.

part of Figure 6b shows the region where the vertical channels are tapered to match the serial register pitch. The V-shaped region is a possible source of unwanted hole collection in the sense region and was designed to incorporate a buried-channel implant to attract holes that are then clocked to a "dump drain" where they are removed.

Measurements at Fermilab[2] showed 15 out of 16 working channels on a thick CCD completely fabricated at Teledyne DALSA Semiconductor. The average read noise for 850 samples was 0.130 ± 0.011 e$^-$ rms, and the range was 0.11 to 0.15 e$^-$ rms. The improvement in readout speed when compared to the standard dark-matter CCDs trivially scales as the ratio of the number of amplifiers per CCD assuming the same number of pixels per device.

The second method investigated for faster readout speeds is loosely based on the distributed floating-gate amplifier concept mentioned previously in Section 4 (Wen et al. 1975; Wen & Salsbury 1973). In that work as well as

[2]Data courtesy of E. Marrufo Villalpando (University of Chicago).

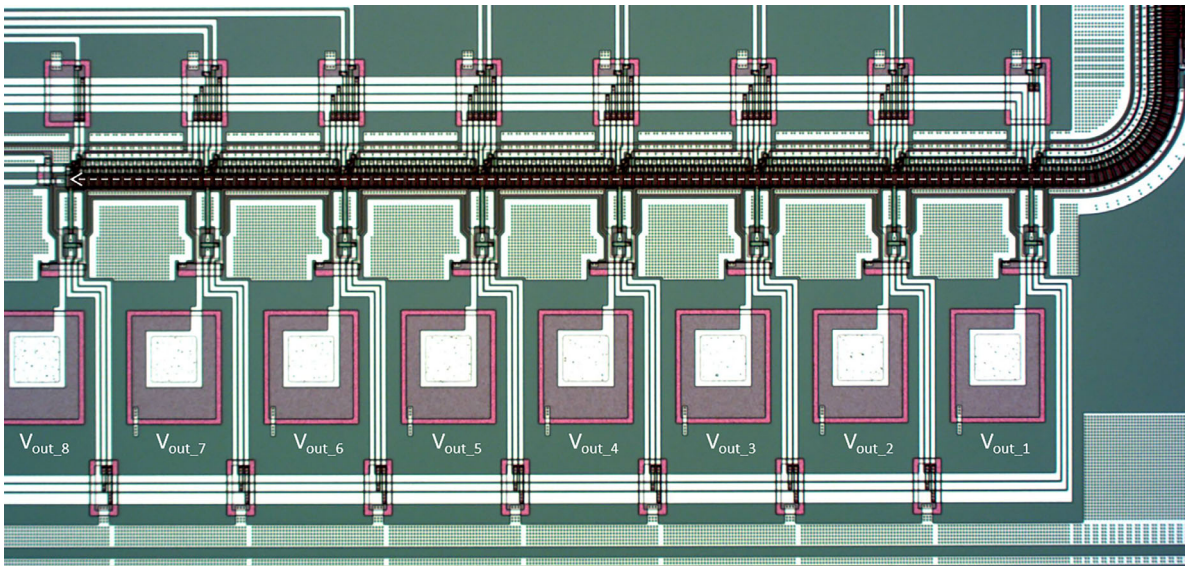

FIGURE 7 A picture of an output region of a fully depleted CCD with 8 individual Skipper CCD amplifiers that are labeled V_{out_1} through V_{out_8}. The direction of the serial readout is shown by the dashed line. For scale, the square Al bond pads just above the labels (white in the image) are 100 μm × 100 μm. In terms of the wafer layout shown in Figure 6, all CCDs not labeled are of the multiple-amplifier sensing type.

a later proposal (Hynecek 1997), the charge was shifted along a serial register with multiple floating-gate sense nodes. The floating-gate sense nodes were connected to charge amplifiers, and the outputs of the charge amplifiers were injected into the output serial register where the signals were summed. Conceptually the final output signal was proportional to $M \times G \times Q_{\text{signal}}$ where M is the number of amplifiers, G is the gain of the charge amplifiers, and Q_{signal} is the original signal level in electrons. A specific implementation is shown in (Wen et al. 1975).

In our approach, we dispense with the charge amplifiers and simply transfer the charge along a serial register with M amplifiers. An implementation with 8 amplifiers is shown in Figure 7. The key assumption is that if the individual reads are statistically independent, then one can reduce the noise by the factor $1/\sqrt{M}$ by simply averaging the measurement results from each amplifier. That is assuming a single read per amplifier for simplicity. Multiple sensing at each amplifier is of course also straightforward.

At first glance, one might consider a major source of error in this approach to be the challenge of accurately determining the amplifier characteristics including the charge-to-voltage conversion factors and the offsets of the individual amplifiers. However, the Skipper CCDs in single-electron counting mode allows for the precise determination of the charge-to-conversion gain and offset. For example, the amplifiers can be calibrated using a low-light signal as in Figure 5a.

The preliminary measurements at Fermilab are encouraging in terms of the noise reduction seen by averaging the results from the individual amplifiers.[3] The improvement in readout speed with this approach goes approximately as $1/M$ when comparing the multiple-amplifier sensing (MAS) approach to that of a single Skipper amplifier. Intuitively, once the first pixel is read out by the Mth amplifier, the following pixel has been read out $M-1$ times.

In more detail, we consider a MAS CCD with M Skipper amplifiers in series. We define N as the number of nondestructive reads, t_{read} as the time to perform one nondestructive read, t_{shift} the time needed to shift the charge by one serial pixel, k_{ex} the number of extended serial pixels, and k_{iAmp} the number of inter-amplifier serial pixels, that is, the number of serial pixels between adjacent amplifiers. Once the charge is shifted into the serial register, the time required to read the first pixel t_1 is given by

$$t_1 = k_{\text{ex}} t_{\text{shift}} + M\left(k_{\text{iAmp}} t_{\text{shift}} + N t_{\text{read}}\right). \quad (1)$$

The total number of reads per charge packet for this case is $M \times N$.

At the time t_1, the second pixel has been read $M-1$ times, and only the time needed to shift the charge packet to the final amplifier plus that required for N reads is necessary to complete the readout of this pixel. It then follows

[3] Personal communication, G. Moroni of Fermilab.

that the general equation for the time t_n to read one row consisting of n serial pixels is

$$t_n = t_1 + \sum_{n=2}^{n} \left(k_{\mathrm{iAmp}} t_{\mathrm{shift}} + N t_{\mathrm{read}} \right) \tag{2}$$

which is simply given by

$$t_n = t_1 + (n-1) \left(k_{\mathrm{iAmp}} t_{\mathrm{shift}} + N t_{\mathrm{read}} \right). \tag{3}$$

The time to read an array of n columns and m rows is m multiplied by the sum of t_n and the row shift time, but for the purposes of comparison of the different CCDs here one only needs to calculate the readout time for one row. For the MAS-type CCDs, each charge packet is measured $M \times N$ times.

For a conventional Skipper CCD with one amplifier per serial register, the time needed to read out a row of n pixels with each charge packet sampled $M \times N$ times would be

$$t_{Cn} = k_{\mathrm{Cex}} t_{\mathrm{shift}} + n \left(t_{\mathrm{shift}} + MN t_{\mathrm{read}} \right), \tag{4}$$

where k_{Cex} is the number of extended serial pixels for the conventional Skipper CCD with one amplifier per serial register.

In order to derive a simple readout-scaling comparison, we neglect the first terms in Equations (3) and (4). The ratio of the readout times is then

$$t_n / t_{Cn} = (n-1) \left(k_{\mathrm{iAmp}} t_{\mathrm{shift}} + N t_{\mathrm{read}} \right) / \left[n \left(t_{\mathrm{shift}} + MN t_{\mathrm{read}} \right) \right]. \tag{5}$$

In general MNt_{read} is much greater than t_{shift}, and if we can neglect the time to shift the charge between the MAS amplifiers when compared to Nt_{read}, then the ratio t_n/t_{Cn} goes as the inverse of the number of MAS amplifiers M.

The practical limitation to the number of on-chip Skipper amplifiers is the number of external readout channels required. The ability to reduce the single-read noise for the Skipper CCD floating-gate amplifiers would reduce the number of samples required for a given noise level, and this is a promising area of research for further reductions in the readout time for Skipper CCDs. The readout electronics used in this work are described in (Moroni et al. 2019).

Referring again to Figure 6a, the 6144 (columns) × 1024 (rows) CCD with one amplifier per corner is baselined for a Skipper CCD mosaic focal plane for the SOAR telescope (Villalpando et al. 2022). This will be the first major demonstration of Skipper CCDs for astronomy (Drlica-Wagner et al. 2020). The first back-illuminated CCDs have been produced, and are in the process of packaging and testing at Fermilab. The first two CCDs tested have shown single-electron counting and QE similar to the DESI CCDs. Four science-grade CCDs are required for the instrument. The CCD is of the same format as one of the two SENSEI CCDs shown in Figure 5b.

6 | OTHER WORK

We are also involved in the production of CCDs for radiation detection applications, and the technology transfer of the LBNL fully depleted CCD technology to 200 mm-diameter wafer foundries.

6.1 | CCDs for radiation detection

A group at the DOE Pacific Northwest National Laboratory (PNNL) has explored the use of DAMIC R&D prototype CCDs for fundamental radiation studies. For this application, a high dynamic range is desirable in order to span the detection of low-energy particles such as the β electron from ^{3}H up to particles with large energy depositions, for example, the 5.5 MeV α-particle from Rn.

Figure 8 shows a spectrum measured at PNNL[4] from a source containing ^{133}Xe and ^{131m}Xe. The spectrum shows the detection of conversion electrons (CE) as well as x and γ rays. A notable feature in the spectrum is the γ-ray at about 81 keV. The probability of absorption for an 80 keV γ ray is about a tenth of a percent for 20 μm of silicon but rises to about 3.3% for the 650 μm CCD used in this work.

We have recently produced thick, back-illuminated CCDs for the Gaseous Radioisotope Analysis In Situ Laboratory (GRAIL) project. The 650 μm-thick wafers were thinned to 580 μm to remove the thick "dead layer" on the back of the CCD. The several-micron thick "dead layer" is opaque to low-energy particles with short absorption depths in silicon, and results from backside films deposited in the CCD process as well as a thick doped region due to P-diffusion from the gettering layer. Starting from the back surface of the silicon, the films are Si_3N_4 and 3 or 4 alternating layers of polysilicon and SiO_2 depending on the process flow used at Teledyne DALSA Semiconductor (Aguilar-Arevalo et al. 2022a). By removing the dead layer and replacing it with a 20–30 nm thick in-situ doped polysilicon layer, we have demonstrated the detection of low-energy β electrons from ^{3}H down to about 2 keV (to be published). As part of the GRAIL project CCDs with a 10 nm, Sb-doped molecular-beam epitaxy (MBE) layer on the back sides of the wafers were also realized. The MBE work was done at MIT Lincoln Laboratory.

[4]Data courtesy of T. Hossbach, PNNL.

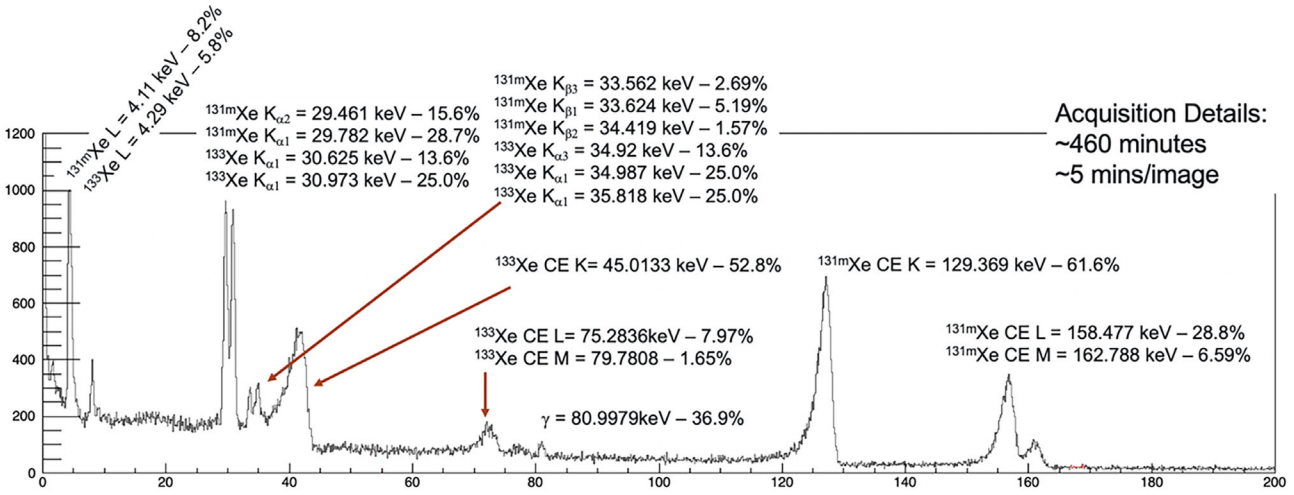

FIGURE 8 The spectrum from a source containing ^{133}Xe and ^{131m}Xe measured with a 650 μm fully depleted CCD. CE refers to conversion electrons.

The dark-matter projects would also benefit from CCDs with thin backside layers. For dark-matter detection, the reduction of events from environmental backgrounds is critical. For example, Rn on the surface of the CCD acts as a source of low-energy β electrons. In (Moroni et al. 2021), the ^{55}Fe spectrum measured for CCDs with the thick dead layer showed a featureless low-energy spectrum due to partial charge collection from some fraction of the x-ray events, whereas an astronomy CCD with anti-reflection coatings and the thin in-situ doped polysilicon layer had much improved low-energy response due to less electron-hole pair recombination. Also, the polysilicon backside films present in the Teledyne DALSA Semiconductor CCDs contain H_2 as a result of the use of hydrides to deposit the films. This includes the in-situ doped polysilicon gettering layer that is deposited by the decomposition of SiH_4 and 1.5% PH_3 in SiH_4. The removal of these films eliminates the production of ^{3}H from the cosmogenic activation of the H_2 in those films (Amaré et al. 2018). However, the thin films on the front sides of the CCDs that are necessary for the proper function of the devices remain a potential source of ^{3}H.

6.2 | CCD development on 200 mm diameter wafers

In 2019 we received a letter from Teledyne DALSA Semiconductor with the heading "NOTIFICATION of DISCONTINUANCE of 150 mm CCD process wafer fabrication." Factors influencing this necessity to cease the operation of the CCD process included the challenge of maintaining a 150 mm CCD-fabrication line with aging equipment, and less revenue from CCD production due to the migration from CCDs to CMOS imagers for Teledyne DALSA Semiconductor's commercial customers. The former issue is also a significant challenge for the LBNL Microsystems Laboratory.

The deadline for the end of foundry CCD fabrication has been extended several times, and we were able to fabricate the dark-matter and QIS CCDs described earlier in the 2019–2022 timeframe. The production of the DAMIC-M CCDs is presently in progress at Teledyne DALSA Semiconductor.

The next-generation Observatory of Skipper CCDs Unveiling Recoiling Atoms (OSCURA) project (Aguilar-Arevalo et al. 2022b; Chierchie et al. 2022) is a 10 kg-scale direct dark matter experiment. R&D funding for OSCURA has enabled the first demonstration of fully depleted CCDs on 200 mm wafers. Key to this work was the ability to procure very high-resistivity silicon from Topsil. The resistivity and lifetimes are given in the last two entries in Table 2. Figure 9 shows 725 μm thick, 200 mm-diameter wafers containing fully depleted CCDs with fabrication at both Microchip Technology and Lincoln Laboratory. The initial results from both entities are promising, and preliminary results for the Microchip Technology CCDs are reported in (Cervantes-Vergara et al. 2023).

The format for the Skipper CCDs fabricated on the 200 mm-diameter wafers is 1058 (columns) × 1278 (rows) with (15 μm)^2 pixels. The size was chosen to fit within the 21.5 mm × 21.5 mm field size for the step-and-repeat photolithography equipment that is standard at 200 mm-wafer semiconductor fabrication facilities. The CCD is smaller in the column direction in order to accommodate LBNL-designed test structures that include 2 and 10 mm^2 diodes to monitor the dark current.

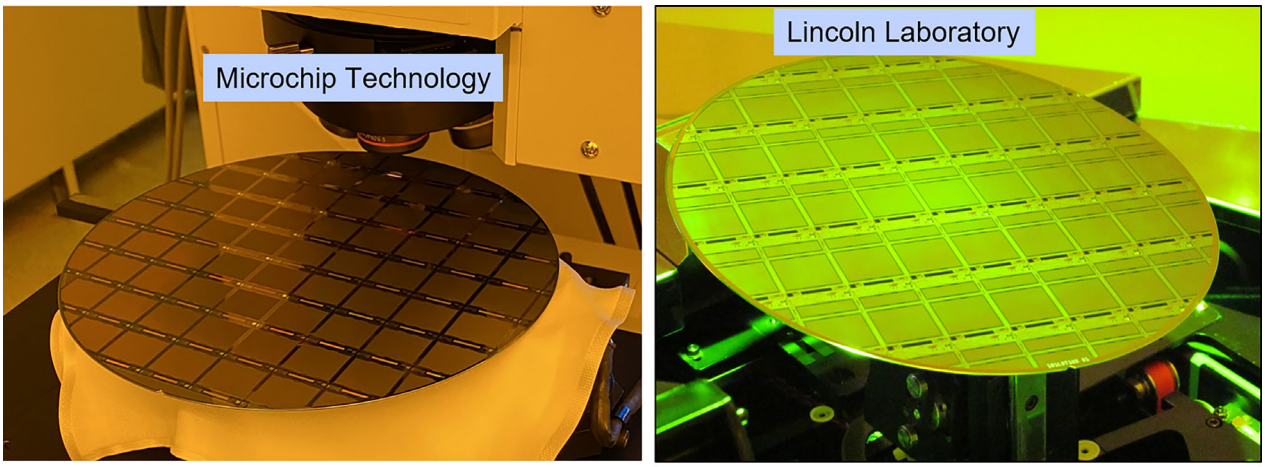

FIGURE 9 Pictures of 200 mm-diameter wafers fabricated at (a) Microchip Technology (b) Lincoln Laboratory. The fully depleted CCDs have a format of 1058 (columns) ×1278 (rows) with (15 μm)^2 pixels, and the wafer thickness is 725 μm.

The change from the 150 mm 1*x* projection photolithography where full-wafer layouts are possible to the step-and-repeat methods used in the 200 mm facilities is a paradigm shift. The ability to produce many different types of CCDs on a wafer as in Figure 4b is no longer viable with the 200 mm technology, and large-format CCDs of the size of the DECam and DESI CCDs require stitching methods (Holland 1992; Pool et al. 1990; Theuwissen 1998; Theuwissen et al. 1998). We expect to produce stitched, fully depleted CCDs in the near future.

7 | CONCLUSIONS

We have presented a review as well as the present status of our development of fully depleted CCDs. The applications have gone beyond astrophysics and into direct dark matter and fundamental radiation detection. The latter applications benefit from the realization of fully depleted CCDs that can be as thick as 725 μm, the standard thickness of a 200 mm wafer. The production of fully depleted Skipper CCDs with sub-electron read noise has resulted in operational as well as in-construction and planned dark-matter experiments with each successive project proposing an order of magnitude increase of detector mass when compared to that of the previous experiment. The ability to increase the readout speed of Skipper CCDs will likely lead to new applications, and we are exploring methods to do this.

ACKNOWLEDGMENTS

This research is supported by the Director, Office of Science, Office of High Energy Physics of the U.S. Department of Energy under Contract No. DE–AC02–05CH11231, the Office of the Director of National Intelligence under Contract No. D2021-2108030006, the U.S. Department of Energy sponsor awards with Battelle (PNNL) and Fermi Research Alliance, LLC, the University of Chicago under Contract No. FP00011073, and the University of Washington under Contract No. FP00006742.

ORCID

Stephen E. Holland https://orcid.org/0000-0001-7218-3457

REFERENCES

Abareshi, B., Aguilar, J., Ahlen, S., et al. 2022, *Astron. J.*, *164*(5), 207. https://doi.org/10.3847/1538-3881/ac882b.

Aguilar-Arevalo, A., Amidei, D., Arnquist, I., et al. 2022a, *Phys. Rev. D.*, *105*, 62003. https://doi.org/10.1103/PhysRevD.105.062003.

Aguilar-Arevalo, A., Amidei, D., Bertou, X., et al. 2015, *J. Instrum.*, *10*(8), P08014. https://doi.org/10.1088/1748-0221/10/08/P08014.

Aguilar-Arevalo, A., Bessia, F. A., Avalos, N., et al. 2022b, *Oscura Exp.* https://arxiv.org/abs/2202.10518.

Amaré, J., Castel, J., Cebrián, S., et al. 2018, *Astropart. Phys.*, *97*, 96. https://www.sciencedirect.com/science/article/pii/S0927650517301895.

Arnquist, I., Avalos, N., Bailly, P., et al. 2022, The DAMIC-M Experiment: Status and First Results. https://arxiv.org/abs/2210.12070.

Barak, L., Bloch, I. M., Botti, A., et al. 2022, *Phys. Rev. Appl.*, *17*, 014022 https://link.aps.org/doi/10.1103/PhysRevApplied.17.014022.

Barak, L., Bloch, I. M., Cababie, M., et al. 2020, *Phys. Rev. Lett.*, *125*, 171802. https://link.aps.org/doi/10.1103/PhysRevLett.125.171802.

Barreto, J., Cease, H., Diehl, H., et al. 2012, *Phys. Lett. B*, *711*(3), 264. https://www.sciencedirect.com/science/article/pii/S0370269312003887.

Bebek, C., Emes, J., Groom, D., et al. 2017, *J. Instrum.*, *12*(4), C04018. https://doi.org/10.1088/1748-0221/12/04/C04018.

Bebek, C. J., Coles, R. A., Denes, P., et al. 2012, in: *High Energy, Optical, and Infrared Detectors for Astronomy V*, eds. A. D. Holland & J. W. Beletic, Vol. *8453*, SPIE (Amsterdam, The Netherlands), 845305. https://doi.org/10.1117/12.926606.

Cervantes-Vergara, B., Perez, S., D'Olivo, J., et al. 2023, *Nucl. Instrum. Methods Phys. Res., Sect. A*, *1046*, 167681. https://www.sciencedirect.com/science/article/pii/S0168900222009731.

Chandler, C. E., Bredthauer, R. A., Janesick, J. R., & Westphal, J. A. 1990, in: *Charge-Coupled Devices and Solid State Optical Sensors*, ed. M. M. Blouke, Vol. *1242*, SPIE (Santa Clara, CA), 238. https://doi.org/10.1117/12.19457.

Chierchie, F., Chavez, C. R., Haro, M. S., et al. 2022, First results from a multiplexed and massive instrument with sub-electron noise Skipper-CCDs. https://arxiv.org/abs/2210.16418.

Claeys, C., & Simoen, E. 2018, *Metal Impurities in Silicon- and Germanium-Based Technologies: Origin, Characterization, Control, and Device Impact*, Springer International Publishing (Cham), 351. https://doi.org/10.1007/978-3-319-93925-4_8.

Dey, A., Rabinowitz, D., Karcher, A., et al. 2016, in: *Groundbased and Airborne Instrumentation for Astronomy VI*, eds. C. J. Evans, L. Simard, & H. Takami, Vol. *9908*, SPIE (Edinburgh), 99082C. https://doi.org/10.1117/12.2231488.

Diehl, H. T. (2020), https://www.osti.gov/biblio/1596042

Drlica-Wagner, A., Villalpando, E. M., O'Neil, J., et al. 2020, in: *X-Ray, Optical, and Infrared Detectors for Astronomy IX*, eds. A. D. Holland & J. Beletic, Vol. *11454*, SPIE, 114541A. https://doi.org/10.1117/12.2562403.

Du, P., Egana-Ugrinovic, D., Essig, R., & Sholapurkar, M. 2022, *Phys. Rev. X*, *12*, 011009. https://link.aps.org/doi/10.1103/PhysRevX.12.011009.

Estrada, J., Cease, H., Diehl, H. T., Flaugher, B., Jones, J., Kubik, D., & Sonnenschein, A. 2008, Prospects for a direct dark matter search using high resistivity CCD detectors. https://arxiv.org/abs/0802.2872.

Fairfield, J. A., Groom, D. E., Bailey, S. J., et al. 2006, *IEEE Trans. Nucl. Sci.*, *53*(6), 3877. https://doi.org/10.1109/TNS.2006.885793.

Fernández Moroni, G., Estrada, J., Cancelo, G., Holland, S. E., Paolini, E. E., & Diehl, H. T. 2012, *Exp. Astron.*, *34*, 43. https://doi.org/10.1007/s10686-012-9298-x.

Flaugher, B., Diehl, H. T., Honscheid, K., et al. 2015, *Astron. J.*, *150*(5), 150. https://doi.org/10.1088/0004-6256/150/5/150.

Groom, D. E., Haque, S., Holland, S. E., & Kolbe, W. F. 2017, *J. Appl. Phys.*, *122*(5), 055301. https://doi.org/10.1063/1.4986506.

Groom, D. E., Holland, S. E., Levi, M. E., Palaio, N. P., Perlmutter, S., Stover, R. J., & Wei, M. 1999, in: *Sensors, Cameras, and Systems for Scientific/Industrial Applications*, eds. M. M. Blouke & G. M. W. Jr, Vol. *3649*, SPIE (San Jose, CA), 80. https://doi.org/10.1117/12.347079.

Grove, A. 1967, *Physics and Technology of Semiconductor Devices*, John Wiley and Sons (New York).

Holland, S. 1989, *Nucl. Instrum. Methods Phys. Res., Sect. A*, *275*(3), 537 https://www.sciencedirect.com/science/article/pii/0168900289907419.

Holland, S. 1992, *IEEE Trans. Nucl. Sci.*, *39*(5), 1259. https://doi.org/10.1109/23.173187.

Holland, S., Bebek, C., Daniels, P., et al. 2007a, *2007 IEEE Nuclear Science Symposium Conference Record*, IEEE (Honolulu, HI), Vol. *3*, 2220. https://ieeexplore.ieee.org/document/4436592.

Holland, S., Dawson, K., Palaio, N., Saha, J., Roe, N., & Wang, G. 2007b, *Nucl. Instrum. Methods Phys. Res., Sect. A*, *579*(2), 653 https://www.sciencedirect.com/science/article/pii/S0168900207011564.

Holland, S., Groom, D., Palaio, N., Stover, R., & Wei, M. 2003, *IEEE Trans. Electron Devices*, *50*(1), 225.

Holland, S. E., Bebek, C. J., Dawson, K. S., et al. 2006, in: *High Energy, Optical, and Infrared Detectors for Astronomy II*, eds. D. A. Dorn & A. D. Holland, Vol. *6276*, SPIE (Orlando, FL), 62760B. https://doi.org/10.1117/12.672393.

Holland, S. E., Bebek, C. J., Dion, F., Frost, R., Groulx, R., Lee, J. S., & Wang, G. 2014, in: *High Energy, Optical, and Infrared Detectors for Astronomy VI*, eds. A. D. Holland & J. Beletic, Vol. *9154*, SPIE (Montréal, Canada), 91541E. https://doi.org/10.1117/12.2057219.

Holland, S. E., Kolbe, W. F., & Bebek, C. J. 2009, *IEEE Trans. Electron Devices*, *56*(11), 2612. https://ieeexplore.ieee.org/document/5280320.

Hynecek, J. 1997, *IEEE Trans. Electron Devices*, *44*(10), 1679. https://doi.org/10.1109/16.628823.

Janesick, J. R., Elliott, T. S., Dingiziam, A., Bredthauer, R. A., Chandler, C. E., Westphal, J. A., & Gunn, J. E. 1990, in: *Charge-Coupled Devices and Solid State Optical Sensors*, ed. M. M. Blouke, Vol. *1242*, SPIE, 223. (Santa Clara, CA, United States). https://doi.org/10.1117/12.19452.

Kassis, M. F., Allen, S., Alvarez, C., et al. 2022, in: *Ground-Based and Airborne Instrumentation for Astronomy IX*, eds. C. J. Evans, J. J. Bryant, & K. Motohara, Vol. *II*, *12184*, SPIE, 1218405. https://doi.org/10.1117/12.2628630.

Moroni, G. F., Andersson, K., Botti, A., Estrada, J., Rodrigues, D., & Tiffenberg, J. 2021, *Phys. Rev. Appl.*, *15*, 064026-1 – 064026-9. https://link.aps.org/doi/10.1103/PhysRevApplied.15.064026.

Moroni, G. F., Chierchie, F., Haro, M. S., et al. 2019, *2019 Argentine Conference on Electronics (CAE)*, 86, IEEE (Mar del Plata, Argentina), 064026-1. https://doi.org/10.1109/CAE.2019.8709274.

Pool, P. J., Suske, W. A., Ashton, J. E., & Bowring, S. R. 1990, in: *Charge-Coupled Devices and Solid State Optical Sensors*, ed. M. M. Blouke, Vol. *1242*, SPIE (Santa Clara, CA), 17. https://doi.org/10.1117/12.19428.

Smith, A. R., McDonald, R. J., Hurley, D. C., et al. 2002, in: *Sensors and Camera Systems for Scientific, Industrial, and Digital Photography Applications III*, eds. N. Sampat, J. Canosa, M. M. Blouke, et al., Vol. *4669*, SPIE (Santa Clara, CA), 172. https://doi.org/10.1117/12.463423.

Theuwissen, A. 1998, *28th European Solid-State Device Research Conference*, IEEE (Bordeaux, France), 56. https://doi.org/10.1117/12.304567.

Theuwissen, A. J. P., Beenhakkers, M., Dillen, B. G. M., et al. 1998, in: *Solid State Sensor Arrays: Development and Applications II*, ed. M. M. Blouke, Vol. *3301*, SPIE (San Jose, CA), 37. https://doi.org/10.1117/12.304567.

Tiffenberg, J., Sofo-Haro, M., Drlica-Wagner, A., et al. 2017, *Phys. Rev. Lett.*, *119*, 131802. https://link.aps.org/doi/10.1103/PhysRevLett.119.131802.

Villalpando, E. M., Drlica-Wagner, A., Bonati, M., et al. 2022, in: *XRay, Optical, and Infrared Detectors for Astronomy X*, eds. A. D.

Holland & J. Beletic, Vol. *12191*, SPIE (Montréal, Canada), 121910U. https://doi.org/10.1117/12.2629475.

Wen, D. 1974, *IEEE J. Solid State Circuits*, *9*(6), 410. https://doi.org/10.1109/JSSC.1974.1050535.

Wen, D., Early, J., Kim, C., & Amelio, G. 1975, *1975 IEEE International Solid-State Circuits Conference*, Vol. *XVIII*, Digest of Technical Papers, Philadelphia, PA, 24. https://doi.org/10.1109/ISSCC.1975.1155402.

Wen, D., & Salsbury, P. 1973, *1973 IEEE International Solid-State Circuits Conference. Digest of Technical Papers*, Philadelphia, PA, Vol. *XVI*, 154. https://doi.org/10.1109/ISSCC.1973.1155181.

AUTHOR BIOGRAPHY

Stephen E. Holland is a Senior Engineer at the Lawrence Berkeley National Laboratory. He received the Ph.D. degree in electrical engineering from the University of California, Berkeley in 1986.Since 1987 he has been with the Lawrence Berkeley National Laboratory. Dr. Holland is a member of the Institute of Electrical and Electronics Engineers and is a Fellow of the American Physical Society. He was awarded the IEEE Nuclear and Plasma Sciences Society Merit Award in 2001, received a Lifetime Achievement Award at the 2013 Scientific Detectors Workshop, and was the co-recipient of the APS Division of Particles and Fields Instrumentation Award in 2016.

How to cite this article: Holland, S. E. 2023, *Astron.Nachr./AN*, e20230072. https://doi.org/10.1002/asna.20230072